Indian Journal of Chemistry
Vol. 58A, April 2019, pp. 454-458

Notes

Synthesis, characterization and properties of nickel based zinc ferrite nanoparticles

Hemant Kumar Dubey[a], Chanda Verma[a], U S Rai[b], Atendra Kumar[c] & Preeti Lahiri[a,*]

[a]Department of Chemistry, MMV, Banaras Hindu University, Varanasi 221 005, India

[b]Department of Chemistry, Institute of Science, Banaras Hindu University, Varanasi 221 005, India

[c]Department of Chemistry, Indian Institute of Technology, Banaras Hindu University, Varanasi 221 005, India

Email: plahiri16@yahoo.com

Received 17 July 2018; accepted 28 March 2019

A cost effective and environmental friendly sol-gel auto-combustion technique has been used to synthesize spinel ferrite nanoparticles of $Ni_xZn_{1-x}Fe_2O_4$ (x = 0.0, 0.5 and 1.0). They were characterized by X-ray diffraction (XRD), Fourier transform infrared spectroscopy (FTIR), scanning electron microscopy (SEM) and Energy dispersive X-ray spectroscopy (EDX). While their magnetic properties have been measured at room temperature using a Magnetic Properties Measurement System (MPMS) quantum design magnetometer, the LCR meter (PSM 1735, NumetriQ 4th Ltd U.K.) has been used to study their dielectric properties with variable frequency in the range, 1 Hz–5 MHz. The XRD analysis suggests the presence of cubic spinel structure of ferrites with an average crystallite size of 45–79 nm. The dielectric constant and loss tangent of the samples show a normal dielectric behavior. The variation of dielectric behavior with the frequency is due to the Maxwell-Wagner type interfacial polarization and hopping of electrons between the Fe^{2+} and Fe^{3+} ions. The magnetic studies reveal that addition of Zn^{2+} drastically affects the magnetic properties.

Keywords: Sol-gel method, X-ray diffraction**,** Magnetic properties, Dielectric

With a view to obtain potential chemical stability, low magnetic coercivity, moderate saturation magnetization, high permeability, high electrical resistivity and low eddy current; a significant progress in the synthesis and characterization of spinel ferrite nanoparticles, has been witnessed recently. The recent possibility of preparing ferrites in the form of nanoparticles has opened a new research field of electronic technology as well as biotechnology[1]. Cubic spinel ferrites with AB_2O_4 formula, crystallize with a face centered cubic structure. Generally spinel ferrites display low magnetic anisotropy and are magnetically soft due to their low coercive field. In recent years, nanoparticle ferrites with a high surface to volume ratio have gained much attention due to their useful electrical and magnetic properties and have been used in magnetic fluids, for information storage and medical diagnostics[2-4]. Ni-Zn ferrite is one of the most promising candidates used in electronics, among other applications. In the inverse spinel structure of $NiFe_2O_4$, the tetrahedral sites are occupied by ferric ions and octahedral sites by ferric and nickel ions. $Ni_{1-x}Zn_xFe_2O_4$ ferrites are ferrimagnetic materials with a large number of technological applications in transformers, antenna, video magnetic heads and magnetic heads of multiple path communication. Furthermore, it has also potential applications in magnetic liquid absorbing materials. Ni-Zn ferrites are among the most widely used soft magnetic materials because of high frequency applications as they posses high magnetic permeability, high electrical resistivity, low eddy current losses and low dielectric[5-8].

Spinel ferrites have been synthesized at nanoscale level by employing various chemical routes such as sol-gel[8], co-precipitation[9], reverse micelle[10], ultrasonication[11], and hydrothermal methods[12]. Among these, the sol-gel method is highly preferable for preparation of ferrites because of their easy preparation, composition, flexibility, and homogeneity[13]. However, there is no report where a systematic work on various aspects of Ni-Zn ferrite system has been found. In the present work, we investigate the effect of adding non-magnetic zinc ions, on the structural and magnetic properties of nickel ferrite nanoparticles. The nanoparticles of Ni-Zn ferrites, $Ni_xZn_{1-x}Fe_2O_4$ (x = 0.0, 0.5 and 1.0) have been synthesized using the sol-gel method. They are characterized by X-ray diffraction (XRD), scanning electron microscopy (SEM), EDX and Fourier transform infrared spectroscopy (FTIR). Their magnetic and dielectric properties along with their dependence on different parameters are also reported.

Experimental

Analytical grade reagents (S D Fine-Chem Ltd) with a high purity of nickel nitrate [$Ni(NO_3)_2.6H_2O$], iron nitrate [$Fe(NO_3)_3.9H_2O$], zinc nitrate [$Zn(NO_3)_2.6H_2O$], and citric acid [$C_6H_8O_7.H_2O$] were

used as raw materials to prepare $Ni_{1-x}Zn_xFe_2O_4$ (x = 0.0, 0.5 and 1.0) by sol-gel method. Citric acid $C_6H_8O_7$ acts as a fuel and complexing agent. Metal nitrates and citric acid were dissolved in a minimum quantity of deionized water in 1:1 molar ratio for all compositions. It was placed on a magnetic stirrer at 60 °C to obtain a homogeneous solution. The pH of the solution was adjusted to 7.0 using ammonia solution. The solution was heated to 80–85 °C with continuous stirring to evaporate water. After evaporation of all water molecules, a fluffy gel was formed which burnt with a sooty flame. It was ground into a fine powder in an agate mortar. The powder was then calcined in a muffle furnace at 1073 K for 4 h.

The powder X-ray diffraction pattern of samples were carried out by X-ray diffractometer (Rigaku miniflex 600, Japan) using Cu-Kα radiation (λ = 1.5405 Å) to identify the phase and structure of the annealed samples. To find out the vibrational modes, Fourier transform infrared spectra (FT-IR) were recorded on a PerkinElmer spectrophotometer in the range of wave numbers 400–4000 cm^{-1} using KBr-pressed pellets. The morphology and the compositional analysis of the annealed samples of ferrite nanoparticles were investigated by a scanning electron microscope (ZESS EVO18), equipped with an Energy Dispersive X-ray Analyzer (EDX). Room temperature magnetic properties of Ni-Zn spinel ferrite nanoparticles were measured using a Quantum Design MPMS (Magnetic Properties Measurement System) magnetometer applying magnetic field of 20 kOe. The dielectric properties of Ni-Zn ferrite was measured using LCR meter (PSM 1735, NumetriQ 4th Ltd U.K.) with a variation of frequency in the range, 1Hz–5MHz. for the measurement of dielectric constant of the annealed Ni-Zn ferrite nanoparticles, pressure around 5 ton was applied to form a pellet with 1.1 mm thickness and 12 mm diameter. PVA was used as a binder. The pellets were heated at 773 K for 3 h to remove the binder material. The pellets were finally coated with conductive silver paint.

Results and discussion

The XRD pattern of $Ni_{1-x}Zn_xFe_2O_4$ (x = 0.0, 0.5, 1.0) ferrites in the 2 theta range of 10–80° are shown in Fig. 1. The X-ray diffraction patterns were compared using the standard JCPDS card No. 86-2267 and 22-1012 for the end ferrites $NiFe_2O_4$ and $ZnFe_2O_4$ respectively. All the peaks in the XRD pattern were indexed using Bragg's law, and the reflections (111), (220), (311), (222), (400), (422), (511) and (440) show the formation of a single phase cubic spinel structure with space group Fd3m. The most intense reflection (311) was used to determine the crystallite size of the sample. Various crystalline parameters like lattice constant, unit cell volume, crystallite size (t), X-ray density (d_x) and measured density (d_m), were calculated from XRD data and are given in Table 1. The lattice constant (a) of Ni-Zn nanoparticles was determined from X-ray data analysis using relation[14],

$$a = d\,(h^2 + k^2 + l^2)^{1/2} \quad \ldots(1)$$

where a is the lattice constant, d is interplanar spacing and h, k, l are Millar indices. The lattice constant increases from 8.3368 Å to 8.4363 Å with the addition of zinc in nickel ferrite (Table 1). The increase in lattice constant is attributed to the difference in ionic radii of Ni^{2+} (0.69 Å) and Zn^{2+} (0.74 Å). The average crystallite size (D) was determined from broadening of the respective high intensity peak (311) by using the Debye-Scherrer formula[15-16]

$$D = \frac{0.9\,\lambda}{\beta \cos\theta} \quad \ldots(2)$$

where, D is crystallite size (nm), λ is a wavelength of X-ray, β was measured using the equation, $\beta = (B^2 - b_0{}^2)^{1/2}$, where, B is measured at full width at half maximum (FWHM) of the experimental profile and b_0 is an instrumental broadening. The values of average crystallite size of the samples were calculated and found to be in the range of 43–79 nm. The X-ray density was calculated from the lattice parameter (a) using the formula,

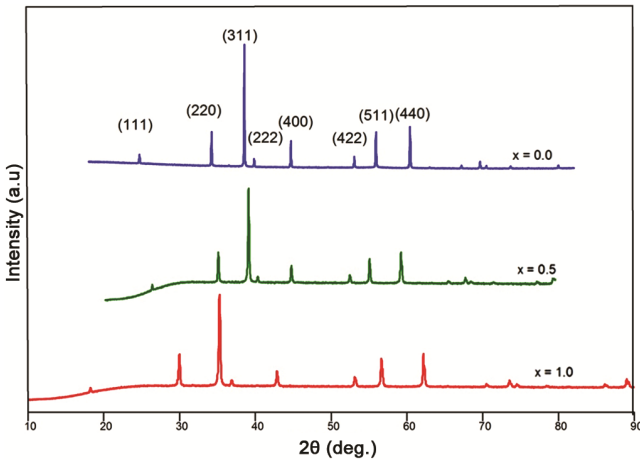

Fig. 1 — Powder X-ray diffraction pattern of $Ni_{1-x}Zn_xFe_2O_4$ (x = 0.0, 0.5, 1.0) ferrite system.

Table 1 — Structural parameters of Ni-Zn ferrite nanoparticles

Sample composition Zn (x)	Lattice constant (Å)	Unit cell volume (cubic Å)	Average crystallite size (nm)	X -ray density (g/cm^3)	Bulk density (g/cm^3)
x = 0.0	8.3368	579.4262	79	5.3396	1.2889
x = 0.5	8.3945	591.5405	43	5.3411	1.3016
x =1.0	8.4363	600.4212	48	5.3727	2.4910

$$d_x = \frac{8M}{Na3} \quad \ldots (3)$$

where, M and N are molecular weight and Avogadro's number, respectively and 8 is the number of molecules per unit cell. The value of d_x increases with increase in zinc substitution and it is attributed to increase in mass that compensates for the decrease in volume. Measured density (d_m) in g cm^{-3} was estimated for each sample from the pellet dimensions using the relation,

$$d_m = \frac{m}{\pi r^2 h} \quad \ldots (4)$$

where, m, r and h are mass, radius and height of the pellet, respectively. In the studied sample of Ni-Zn ferrites the measured density increases with the increase in Zn content because by the substitution of Zn, the volume of the unit cell and the molecular weight of the $Ni_{1-x}Zn_xFe_2O_4$ spinel ferrite increases.

Fourier transform infrared spectroscopy was employed to observe the structural variations and spinel phase of ferrite systems. The FT-IR spectra of the annealed samples of nickel-zinc ferrites are shown in Fig. 2. It has been observed that the spectra consist of two significant absorption bands, first at 600 cm^{-1} and the second at 425 cm^{-1}. Absorption bands observed within this limit reveal the formation of the single phase spinel structure having two sub-lattices, tetrahedral (A) site and octahedral (B) site[17]. The first absorption band observed at 600 cm^{-1} (high frequency ν1) is attributed to the vibration of tetrahedral metal-oxygen bond and the second band at 425 cm^{-1} (low frequency ν2) arises due to stretching vibration of metal-oxygen bond at octahedral sites which confirm the formation of cubic spinel structure[17]. Furthermore, in all samples a band at 1458 cm^{-1} corresponds to antisymmetric NO_3 stretching vibration. Also for x = 1.0 and 0.5, a band observed around 2920–2923 cm^{-1} may be due to C-H stretching bond.

The scanning electron microscopic image of all annealed samples is shown in Fig. 3. It has been observed that the particles have almost homogeneous distribution, and some of them are in an agglomerated

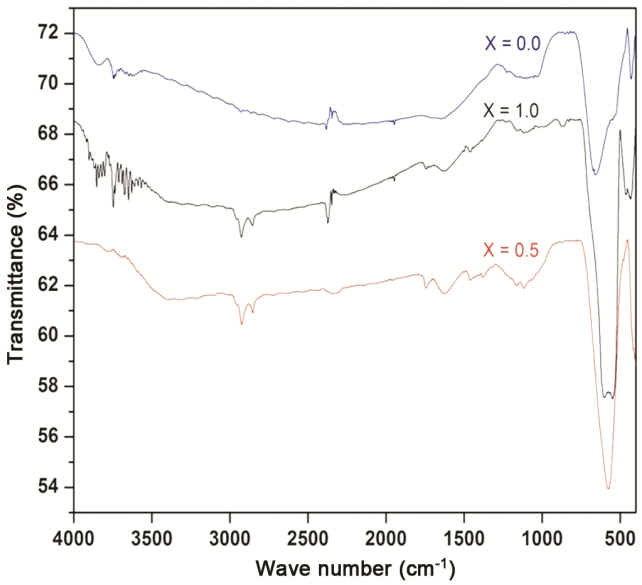

Fig. 2 — FT-IR spectra of $Ni_{1-x}Zn_xFe_2O_4$ (x= 0.0, 0.5, 1.0) ferrite system.

form. The SEM figure clearly indicates that microstructure of grains of sample are ultra-small. Most of the grains containing a large number of atoms have very small dimensions with an average grain size of 10 μm. The compositional analysis of $Ni_{1-x}Zn_xFe_2O_4$ sample was done using energy-dispersive X-ray spectra as shown in Fig. 4. The spectra show the peaks corresponding to Ni, Zn, Fe, and O. The result confirms the absence of impurities in the sample. The data on elemental analysis of all the Ni-Zn nano-ferrite samples with different compositions are given in terms of the weight % and atomic % of different elements in supplementary data, Table S1. An analysis of the compositions of the samples shows a slight difference in the amounts of Zn, Ni, and Fe. However, quantitative ratio of the elements indicates that the compositions of the synthesized materials are close to the stoichiometry of $Ni_{1-x}Zn_xFe_2O_4$.

It has been predicted that in the cubic system of ferromagnetic spinels, the magnetic order is mainly due to a super exchange interaction mechanism occurring between the metal ions in the A and B sub-lattices. The substitution of no-nmagnetic ion such as Zn, which has

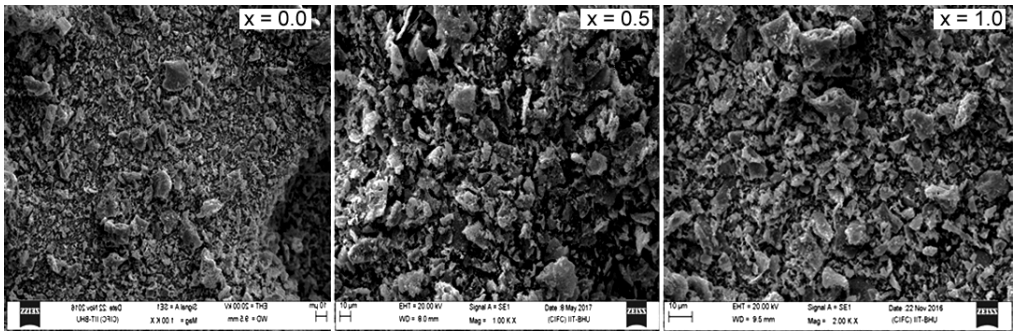

Fig. 3 — SEM images of $Ni_{1-x}Zn_xFe_2O_4$ (x= 0.0, 0.5, 1.0) ferrite system.

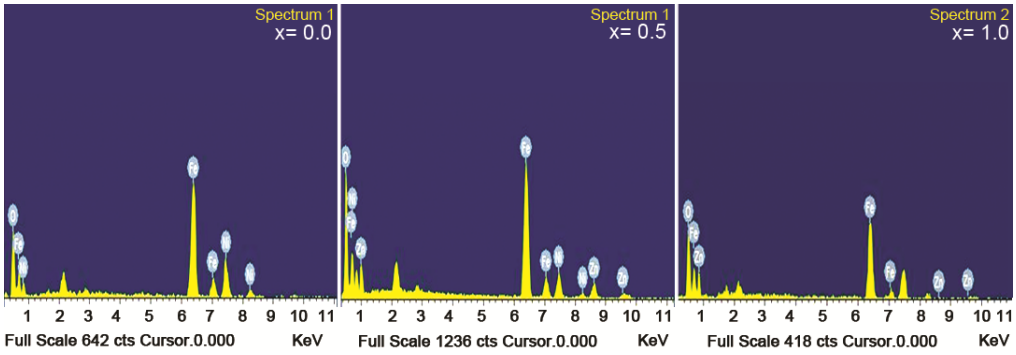

Fig. 4 — EDS images of $Ni_{1-x}Zn_xFe_2O_4$ (x= 0.0, 0.5, 1.0) ferrite system.

a preferential A site occupancy results in the reduction of the exchange interaction between A and B sites. Hence, by varying the degree of zinc substitution, it is possible to vary magnetic properties of the fine particles. The M-H plots of powder samples of $Ni_{1-x}Zn_xFe_2O_4$ ferrite nanoparticles for different zinc concentrations are shown in supplementary data, Fig. S1. It is evident from the figure that the saturation magnetization (Ms) increases and reaches the maximum value of 8.798 emu/g at 9500.38 Oe for x = 0. It is amply clear that the particles do not show any saturation for x = 1.0 and it behaves almost linear. The change in magnetic property, Ms, is due to the influence of the cationic stoichiometry and their occupancy in the specific sites. In addition, formation of dead layer on the surface, existence of random canting of particle surface spins might be the cause for the reduction of magnetic properties of nanoparticles[18,19]. The hysteresis curve recorded at room temperature is typical for a soft magnetic material and indicates hysteresis ferromagnetism.

The value of dielectric constant of ferrite can be calculated by using the following relation

$$\varepsilon = \frac{C_p d}{\varepsilon_0 A} \qquad \ldots(5)$$

where ε_0, d, A and C_p are permittivity of free space, thickness, area of cross-section and measured value of capacitance of the pellet, respectively. The variation of real part of the dielectric constant for $Ni_{1-x}Zn_xFe_2O_4$ as a function of frequency from 1 Hz to 5 MHz at room temperature is shown in Fig. S2a. It is observed that, the dielectric constants decrease with increasing frequency and remain constant at higher frequency. The value of ε is found to be higher at low frequency side with increasing concentration of zinc, which may be due to space charge polarization. On increasing the frequency, the value of dielectric loss (tan δ) for $Ni_{1-x}Zn_xFe_2O_4$ sample, decreases (Fig. S2b). This decrease in tanδ may be due to vacancy of oxygen in the sintered materials. The imaginary part of dielectric constants with frequency at room temperature is shown in Fig. S3. It is observed that for each sample, the dielectric constant decreases with increase in frequency and becomes almost constant at higher frequency. It is well known that the dielectric constant of any material depends on various types of polarizations such as electronic polarization, ionic polarization, dipolar polarization and space charges polarization. The space charge polarization is dominant at low frequency value and the ionic polarization occurs in higher frequency region. The variation of dielectric constant with frequency can be explained on the basis of Maxwell-Wagner polarization model[20-22]. It is well known that, in ferrites with heterogeneous structure the samples

consist of well conducting grains separated by insulating grain boundaries. The electron reach the grain boundary through hopping between $Fe^{2+} \leftrightarrow Fe^{3+}$ ions, so that the electric dipoles align themselves along the applied field, therefore dielectric constant of material is high at low frequency. However, beyond a certain frequency the hopping of electron cannot follow the external field and therefore, the dielectric constant decreases with increasing frequency of the applied field. The dielectric tangent loss can be expressed as

$$\tan\delta = \frac{\varepsilon''}{\varepsilon'} \quad \ldots(6)$$

where δ is the loss angle and ε' and ε'' are real and imaginary part of the dielectric constant, respectively. The frequency dependence of dielectric tangent loss of $Ni_{1-x}Zn_xFeO_4$ (x = 0.0, 0.5, 1.0) ferrites is shown in Fig. S2a. The decrease in dielectric loss tangent with increasing frequency is in accordance with the Koop's phenomenological model. The dielectric loss arises if the polarization lags behind the applied fields and is caused by structural inhomogeneities.

In summary, $Ni_{1-x}Zn_xFe_2O_4$ nanoparticles were prepared successfully using sol-gel method which is an auto combustion technique, convenient for obtaining homogeneous nano size mixed Ni-Zn ferrites. X-Ray diffraction patterns confirm the formation of cubic spinel structure in single phase without any impurity peak. Lattice parameter was found to increase with Zn concentration and this is due to the larger ionic radius of the Zn^{2+} ion in comparison to Ni^{2+}. FT-IR spectrum exhibited expected main absorption bands, thereby confirming the spinel structure. SEM micrograph indicates the particles are in nanometer range and homogeneously distributed. EDX analyses confirm chemical compositions. The room temperature M-H hysteresis curves show that the particles are superparamagnetic at room temperature. The real and imaginary part of dielectric constant decrease with increasing frequency. $NiFe_2O_4$ prepared by sol-gel method shows that it is not a very hard magnetic material since the hysteresis loop is very small and it is known that $ZnFe_2O_4$ is a soft magnetic material. This soft magnetic nanoparticle may have interesting applications, in magnetic coatings and in the preparation of ferrofluids.

Supplementary data

Supplementary data associated with this article are available in the electronic form at http://www.niscair.res.in/jinfo/ijca/IJCA_58A(04)454-458_SupplData.pdf.

Acknowledgement

Authors are grateful to Prof. Rajeev Prakash, in-charge of Central Instrument Facility Center (CIFC) IIT (BHU) for providing instruments facilities.

References

1 Valenzuela R, *Phy Res Int*, 2012 (2012) 1.
2 Arulmurugan R, Jeyadevan B, Vaidyanathan G & Sendhilnathan S, *J Magn Magn Mater* 288 (2005) 470.
3 Mathew D S & Juang R S, *Chem Engg J*, 129 (2007) 51.
4 Lee N, Yoo D, Ling D, Cho M H, Hyeon & Cheon T J, *Chem Rev*, 115 (2015)10637.
5 He X, Song G & Zhu J *Materials Letters*, 59 (2005) 1941.
6 Matsuo Y, Inagaki M, Tomozawa T & Nakao F, *Trans Magn*, 37 *(*2001) 2359.
7 Kumar P S A, Shrotri J J, Kulkarni S D, Deshpande C E & Date S K, *Mater*, 27(1996) 293.
8 Aravind G, Raghasudha M, Ravinder D & Kumar R V, *J Magn Mater*, 406 (2016) 110.
9 Tirupanyam V, Srinivas C, Meena S S,Yusuf S M, Kumar A S, Sastry D L & Seshubai V, *J Magn Magn Mater*, 392 (2015) 101.
10 Gubbala S, Nathani H, Koizol K & Misra R D K, *Phy B,* 348 (2004) 317.
11 Choudhury H A, Choudhary A, Kumar M S & Moholka V S, *Ultrason Sono Chem,* 20 (2013) 294.
12 Bucko M M & Haberko K, *J Eur Ceram Soc*, 27(2007) 723.
13 Aghav P S, Dhage V N, Mane M L, Shengule D R, Dorik R G & Jadhav K M, *Phys B, Cond Matter,* 406 (2011) 4350.
14 Ladgaonkar B P, Bakare P P, Sainkar S R & Vaingankar A S, *Mater Chem Phys*, 69 (2001) 19.
15 Cullity B D, *Elements of X-ray Diffraction* (Addison-Wesley, London) 1959.
16 Klung H P & Alexander L B, *X-ray Diffraction Procedures*, (Wiley, New York) 1974, p. 687.
17 Rendale M K, Mathad S N & Puric V, *Int J Self-Prop High Temp Synth*, 24 (2015) 78.
18 Han D H, Wang J P & Lou H L, *J Magn Magn Mater,* 136 (1994) 176.
19 Kale G M & Asokan T, *Appl Phys Lett,* 62 (1993) 2324.
20 Koops C G, *Physic Rev,* 83 (1951) 121.
21 Maxwell J C, *Electricity and Magnetism* (Oxford University Press, London, UK) 1973.
22 Wagner K W, *Annalen der Physik*, 345 (1913) 817.